HAL
open science

Approaching the Topological Low-Energy Physics of the F Model in a Two-Dimensional Magnetic Lattice

V. Schánilec, O. Brunn, M. Horáček, S. Krátký, P. Meluzín, T. Šikola, Benjamin Canals, N. Rougemaille

To cite this version:

V. Schánilec, O. Brunn, M. Horáček, S. Krátký, P. Meluzín, et al.. Approaching the Topological Low-Energy Physics of the F Model in a Two-Dimensional Magnetic Lattice. Physical Review Letters, 2022, 129 (2), pp.027202. 10.1103/PhysRevLett.129.027202 . hal-03857746

HAL Id: hal-03857746

https://hal.science/hal-03857746v1

Submitted on 17 Nov 2022

HAL is a multi-disciplinary open access archive for the deposit and dissemination of scientific research documents, whether they are published or not. The documents may come from teaching and research institutions in France or abroad, or from public or private research centers.

L'archive ouverte pluridisciplinaire **HAL**, est destinée au dépôt et à la diffusion de documents scientifiques de niveau recherche, publiés ou non, émanant des établissements d'enseignement et de recherche français ou étrangers, des laboratoires publics ou privés.

Approaching the topological low-energy physics of the F-model in a two-dimensional magnetic lattice

V. Schánilec,[1,2] O. Brunn,[1,3,4] M. Horáček,[3] S. Krátký,[3]
P. Meluzín,[3] T. Šikola,[2,4] B. Canals,[1] and N. Rougemaille[1]
[1] *Univ. Grenoble Alpes, CNRS, Grenoble INP, Institut NEEL, 38000 Grenoble, France*
[2] *Central European Institute of Technology, CEITEC BUT, Brno University of Technology, Purkyňova 123, Brno 612 00, Czech Republic*
[3] *Institute of Scientific Instruments of the Czech Academy of Sciences, Královopolská 147, 612 64 Brno, Czech Republic*
[4] *Institute of Physical Engineering, Brno University of Technology, Technická 2, 616 69 Brno, Czech Republic*
(Dated: November 17, 2022)

We demonstrate that the physics of the F-model can be approached very closely in a two-dimensional artificial magnetic system. Faraday lines spanning across the lattice and carrying a net polarization, together with chiral Faraday loops characterized by a zero magnetic susceptibility are imaged in real space using magnetic force microscopy. Our measurements reveal the proliferation of Faraday lines and Faraday loops as the system is brought from low- to high-energy magnetic configurations. They also reveal a link between the Faraday loop density and ice-like spin-spin correlations in the magnetic structure factor. Key for this work, the density of topological defects remains small, of the order of 1% or less, and negligible compared to the density of Faraday loops. This is made possible by replacing the spin degree of freedom used in conventional lattices of interacting nanomagnets by a micromagnetic knob, which can be finely tuned to adjust the vertex energy directly, rather than modifying the two-body interactions.

Introduction– In the beginning of the 20th century, the formulation of the third law of thermodynamics was vigorously debated, notably between Nernst, Planck and Einstein [1–3]. In the 20s, it becomes clear that the following, often taught statement was not precise enough: "When temperature falls to absolute zero, the entropy of a pure crystalline substance tends to a constant, which can be taken to be zero". The heat capacity measurements performed by Giauque and coworkers [4, 5] on water ice were certainly a milestone in that context as they unambiguously demonstrated the existence of an extensive entropy at low temperature. These experimental findings nicely agreed with the description of the proton disorder in ice proposed by Bernal and Fowler [6] and Pauling [7], highlighting solid water as a fascinating candidate for challenging the formulation of the third law.

These works later inspired the introduction in statistical mechanics of the so-called vertex models [8, 9] (see Supplemental Material for details). Although being an abstract, conceptually simple, two-dimensional view of reality, these theoretical approaches proved to be very powerful. Among them, the ice model, one of the variant of the six vertex model, may "be considered to be one of the more successful applications of statistical mechanics to the real world" [10]. The F-model, another variant of the six vertex model, was introduced by Rys in the 60s to describe antiferroelectrics [11], and is one of the few exactly solvable models of statistical mechanics [12–16].

The F-model has rather unusual properties: i) it is characterized by an infinite order phase transition separating a high-temperature critical phase (the so-called square ice) from an antiferromagnetic order, and ii) the configurational space is divided into topological sectors. These properties are inherited from the constraints of the six vertex model, which allows only loop excitations to develop on an antiferromagnetic background consisting of a tessellation of type I vertices (see Fig. 1). These loops are made of type II vertices, whose magnetic moments can be joined into lines (see Fig. 1), the so-called Faraday lines [17]. Faraday lines have a defined A/B parity depending on the plaquettes they bridge (a loop only crosses either A or B plaquettes, see Fig. 1). They carry the system energy [17] and are thus the elementary excitations of the F-model. They are of two kinds: magnetization-free, chiral closed loops extending within the bulk of the lattice, and system-spanning windings, hosting a net magnetization. Only closed loops can be contracted to zero, but they do not couple with an external field as they carry no net magnetization. Instead, system-spanning windings cannot be contracted, forcing the system to fluctuate within

a given topological sector [17, 18].

These theoretically predicted, exotic properties are not easily observed in nature. We might wonder wether they could be conveniently studied experimentally, for example in artificial magnetic systems [19–21], or if this is a lost battle. So far, two-dimensional square assemblies of interacting nanomagnets have failed to probe the topological properties of the F-model, despite the fact that they share the same ground state. As pointed out by Nisoli [17], the transitions in artificial magnetic systems "are innocuously second order [22–25], and their [magnetic] susceptibility is never zero". This is so because the thermodynamics of artificial square ice magnets is described by the *sixteen* vertex model, which permits excitations of vertices violating the ice-rule constraint necessarily satisfied in the *six* vertex model. These ice-rule defects then act as sources or sinks of magnetic flux, breaking the topological properties of the F-model [17].

Here we show that the thermodynamics of the F-model can be approached very closely in a purely two-dimensional system, including its macroscopically degenerate, high-temperature ice regime. More importantly, the topological properties of the F-model can be probed by a careful control of the vertex energies and the reduction of ice-rule defects to a marginal contribution. This allows us to visualize the proliferation of Faraday loop excitations developing on the antiferromagnetic ground state as our system is brought to higher energy configurations. Faraday lines carrying a net magnetization and chiral Faraday loops characterized by a zero magnetic susceptibility are imaged in real space, giving access to the topological properties of the F-model experimentally.

Micromagnetism as an additional degree of freedom– The system we consider is a square lattice of nanomagnets that are physically connected at the vertex sites [see Fig. 2(a)]. The system differs from a conventional artificial square lattice [26] in the sense that it does not consist of an assembly of interacting nanomagnets. Instead, the system can be viewed as a unique object, a magnetic grid, in which the energy results from a micromagnetic texture at the vertex sites rather than a sum of two-body interactions. As we will see below, the energy hierarchy between the four possible vertex types can be tuned by adding a hole at the vertex site, i.e., by extruding some magnetic materials from the grid [see Fig. 2(a)].

To illustrate the influence of the hole diameter on the vertex energies, we first compute the micromagnetic energy [27, 28] of the four possible vertex types [see Fig. 2(b) and Supplemental Material for details on the simulations]. The key result is the capability to change the energy hierarchy between type I and type II ice-rule vertices by varying the hole diameter, while keeping type III topological defects and type IV vertices much higher in energy. The fact that the energies of type I and type II vertices evolve differently as a function of the hole diameter is explained by the change of the microscopic exchange and magnetostatic energies. In the absence of a hole, a type I vertex always costs more energy than a type II vertex [29] as it hosts an antivortex [see Fig. 2(c)], a micromagnetic texture known to be highly energetic because of the exchange penalty resulting form the curl of the magnetization within the core. Type II vertices then have the lowest possible energy in a fully connected grid [29]. For finite hole diameters, the energy of a type II vertex increases because of the additional magnetostatic energy induced by the presence of the hole, while at the same time the exchange penalty is reduced for a type I vertex as the antivortex core is removed [see Fig. 2(c)]. The crossing point where type I and type II vertices have the same energy suggests that the hole diameter can serve as a knob for exploring different variants of the sixteen vertex model. In particular, a Coulomb phase physics should be observed when type I and type II vertices have the same energy.

To test these predictions, we have fabricated a series of square grids made of permalloy, with a material-free circular region at the vertex sites. The grids are 100 nm-wide, 25 nm-thick, and contain

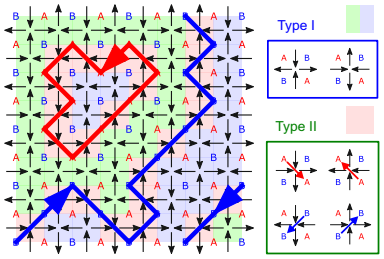

FIG. 1. Schematics showing an excited configuration of the F-model. Type I domains are colored in green and blue, whereas type II vertices appear in red. Only type II vertices carry a magnetic moment which are joined by the Faraday lines (red and blue oriented thick lines). Faraday lines have an assigned parity depending on the A/B plaquettes they bridge (the red Faraday line has A parity and separates neighboring B plaquettes).

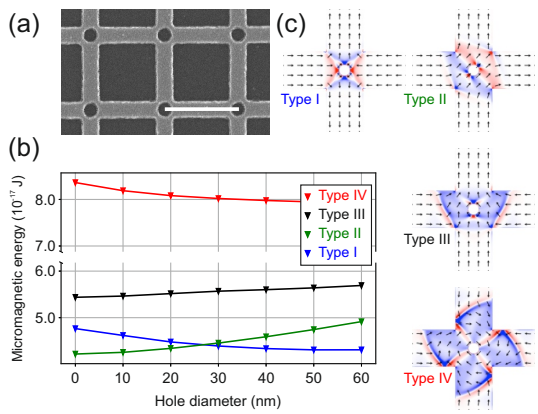

FIG. 2. (a) Electron micrograph of one lattice. Scale bar is 500 nm. (b) Micromagnetic energy of the four vertex types as a function of the hole diameter. (c) Micromagnetic configurations of type I, type II, type III and type IV vertices. Black arrows represent the local direction of magnetization, while the blue / red contrast codes for the divergence of the magnetization vector.

900 vertices (i.e., 1860 pseudo-spins). The vertex-to-vertex distance is set to 500 nm and the hole diameter ϕ is varied between lattices, from 70 to 120 nm, typically (see Supplemental Material for a discussion on the values of the hole diameter). The permalloy grids were field demagnetized and the resulting magnetic configurations are subsequently imaged using a magnetic force microscope (MFM) [see Supplemental Material for details on the demagnetization procedure].

The magnetic configurations of six demagnetized lattices with different hole diameters are reported in Fig. 3(a) (see Supplemental Material for the complete MFM dataset). For large holes ($\phi = 120$ nm), the system is close to the antiferromagnetic ground state configuration built from type I vertices. The two possible degenerate antiferromagnetic domains, shaded in blue and green in Fig. 3(a), are separated by Faraday lines [colored in red and blue in Fig. 3(a)]. As the hole diameter is reduced, the patches of type I domains become smaller, and more type II vertices are observed. Interestingly, for hole diameters of about $\phi = 72$ nm, the populations of type I and type II vertices are comparable to those expected in the square ice manifold (33% and 67%, respectively). These findings indicate that the magnetic correlations can be changed gradually by varying the hole diameter and suggest that micromagnetism can be used as a knob to explore different regimes of the sixteen vertex model. In particular, if properly chosen, the hole diameter could be adjusted to reach the Coulombic spin liquid phase associated with the square ice [30–33].

To confirm this result, we have computed the associated magnetic structure factors (MSF), averaged over four measurements for each hole diameter [Fig. 3(b) and Supplemental Material for the whole dataset]. The MSF analysis indeed shows that tuning the hole diameter allows visualizing several regimes of the sixteen vertex model. For the largest holes, the diffraction pattern is characterized by Bragg peaks at the corners of the Brillouin zone. These Bragg peaks reveal the antiferromagnetic ground state ordering [34]. When reducing the hole diameter, the MSF exhibits a diffuse but structured pattern, typical of the square ice [30, 31]. We thus provide a *purely two-dimensional* artificial system in which to observe both the Coulombic spin liquid of the square ice and the conventional antiferromagnetic order. We emphasize that for each hole diameter, four different lattices are imaged and found to be in a similar state (see Supplemental Material). Our demagnetization protocol allows us reaching efficiently and reproducibly collective low-energy states, consistent with other studies [30, 31]. Finally, recalling that the square ice is the high-temperature regime of the F-model, the question we address next is to what extent the configuration series reported in Fig. 3 can be accounted for by the thermodynamics of the F-model.

Approaching the physics of the F-model– Answering this question first raises the issue of the density of ice-rule defects usually present in artificial systems. Reducing the energy gap between type I and type II ice-rule vertices appears as a necessary but not sufficient condition to avoid trapping topological defects. For example, previous works on square ice systems with a height offset [30–32], or incorporating interaction modifiers [33] show that the monopole density usually remains high, of the order of 10% in field demagnetized arrays [30, 31], when not 20% [32] or more [33] in thermally active systems. Having such a high defect density is detrimental, and all the topological properties of the F-model would be washed out in these previously proposed designs.

The salient feature of our strategy is precisely the fact that the $E_{\mathrm{I}}/E_{\mathrm{II}} \to 1^-$ condition is met (E_{I} and E_{II} standing for the energy of type I and type II vertices, respectively), *while* keeping marginal the density of ice-rule defects. Regardless of the hole diameter, the residual fraction of defects in our lattices

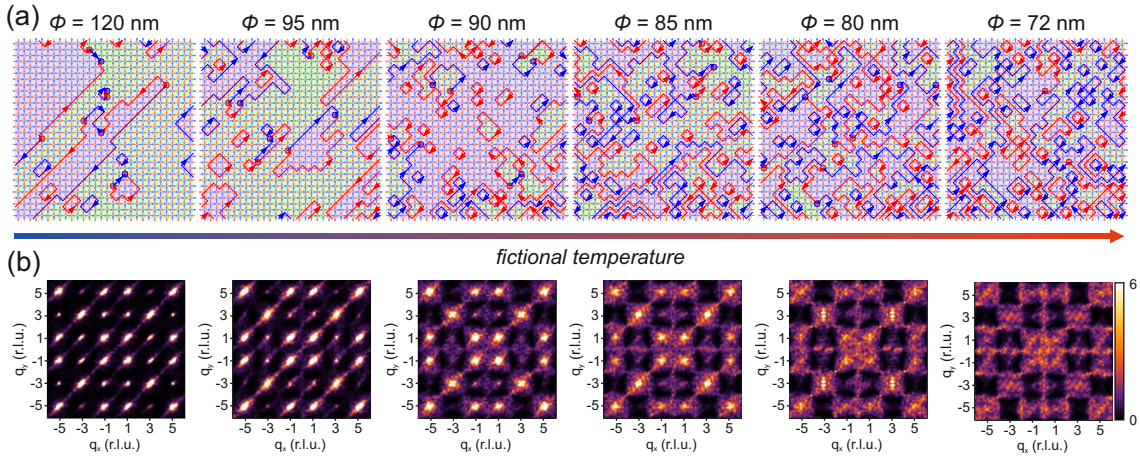

FIG. 3. Real space (a) and reciprocal space (b) analyses of the magnetic configurations obtained after demagnetizing six lattices having different hole diameters ϕ. (a) The two degenerate antiferromagnetic domains are shaded in blue and green. These type I domains are separated by Faraday loops made of type II vertices and represented by directed lines colored in blue and red depending on their parity. Faraday lines having different parities never intersect, except in the presence of an ice-rule defect (shown by a colored open circle). (b) The magnetic structure factors are averaged over four real space configurations (i.e., 3600 vertices / 7440 spins) for each hole diameter to improve statistics, and are calculated for wavevectors covering ± 6 reciprocal lattice units (r.l.u.). Intensity scale is the same in all six MSF.

is 1% typically or less. In particular, in the lattices where the $E_{\mathrm{I}}/E_{\mathrm{II}} \to 1^-$ condition is approached, we are able to image many Faraday loops which are not interrupted by an ice-rule defect (there are typically 10 times more Faraday loops than topological defects when $\phi < 85$ nm). This contrasts with previous literature in which these two quantities are similar, when ice-rule defects are not even in a higher proportion (see for instance Refs. 35–37 and Supplemental Material for a discussion on the defect density).

Describing our experimental results in terms of Faraday loops is thus relevant. Some of the Faraday lines we imaged form closed and chiral loops, extending entirely within the lattice. As predicted, these loops have parity properties [17], and both parities are equally populated in our experiments [see colored histogram in Fig. 4(a)]. Closed loops do not carry any net polarization and then must have zero magnetic susceptibility. Other Faraday lines form open strings spanning across the system and ending at the lattice boundaries. Indeed, because of the finite size of our arrays, the Faraday lines can remain open and anchored at the lattice edges. Many of these lines as well do not host any ice-rule defect, and thus carry a net polarization. Finally, we observe that loops having the same parity can intersect, whereas loops of opposite parity never cross [17].

Analyzing the series of lattices as a whole, two main features are observed. First, the loop density continuously decreases as the hole diameter is increased [see Fig. 4)(a)]. This effect is particularly pronounced for the smallest loops, whose amount drops by more than an order of magnitude through the series [see Fig. 4)(b)]. This is a direct evidence of the contraction of Faraday loops as the system approaches the antiferromagnetic ground state. The second feature is the change of the Faraday loop curvature. Close to the ice regime, the Faraday loops have a meandering shape, whereas they become straighter when type I domains develop. This can be illustrated by plotting the average number of times a loop changes direction [see Fig. 4)(c)]. We interpret this result as a consequence of the ordered background tension which becomes more significant as the effective temperature of the system is reduced.

Interestingly, the magnetic structure factors reported in Fig. 3b also suggest a gradual change of the spin-spin correlations across the lattice series. When $\phi = 72$ nm, the MSF strongly resembles the one of the square ice, i.e., a diffuse but structured background with emerging pinch points. When 80 nm $\leq \phi \leq 90$ nm, the MSFs show the coexistence of an ice-like background and Bragg peaks associated with an antiferromagnetic ordering. The ice-like background becomes fainter as ϕ increases, whereas the Bragg peaks become more intense. Finally, when $\phi \geq 90$

nm, the ice-like background has totally disappeared and the MSFs only exhibit intense Bragg peaks. It is thus tempting to consider the lattice series as an approximate of F-model probed at different fictional temperatures, from the high-temperature correlated ice regime to a low-energy antiferromagnetic state, via several intermediate temperatures.

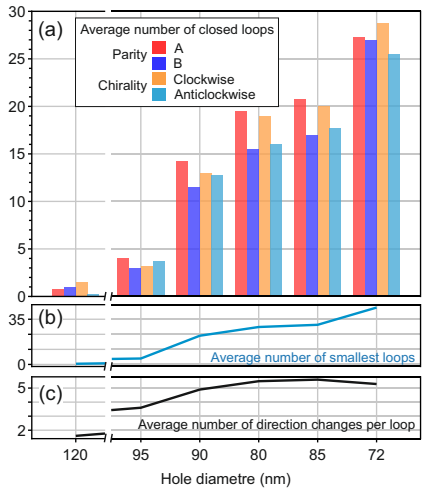

FIG. 4. (a) Average number of closed loops for 24 measured lattices (for each hole diameter, four lattices are analyzed). The loops are characterized by parity and a chirality. Both quantities are equally populated, showing that our demagnetization protocol does not induce any bias. (b) Average number of the smallest possible closed loops. (c) Number of times a loop changes direction on average.

We might argue that the presence of a few ice-rule defects is sufficient to make the system fluctuate and to ultimately order the lattice in a conventional manner, washing out the topological properties of the Faraday lines. We believe this is only partly true when approaching the antiferromagnetic ground state. The main reason is that ice-rule defects have then local dynamics, and the excursions they can make outside their loop are extremely limited. This can be understood by illustrating the motion an ice-rule defect can make in a configuration observed experimentally [see Fig. 5(a)]. The potential moves for the two imaged defects are represented by colored arrows. A red arrow corresponds to a forbidden spin flip event as it generates a highly energetic all-in / all-out state. A green arrow indicates a potential spin flip with no energy cost, i.e., the ice-rule defect is free to move in this direction. A yellow arrows is associated to a motion having a finite energy cost due to the creation of a new type II vertex, thus increasing the loop length. At low enough effective temperature, ice-rule defects are confined within their loop. When they have the opportunity to penetrate into the antiferromagnetic background, they are immediately pushed back into their loop [see Fig. 5(b)]. As a consequence, the few residual ice-rule defects remaining in our lattices are less and less capable to unwind the Faraday loops, and the dynamics is expected to freeze as the ground state is approached. In other words, in our approximate of the F-model, the dynamics stops for two reasons: the single spin flip dynamics freezes as global updates become the only relevant excitations, and the remaining ice-rule defects trapped within the Faraday loops have only local dynamics. We then conclude that the few ice-rule defects we observe experimentally do not affect much the properties of the Faraday loops, and our system is a good approximate of the F-model.

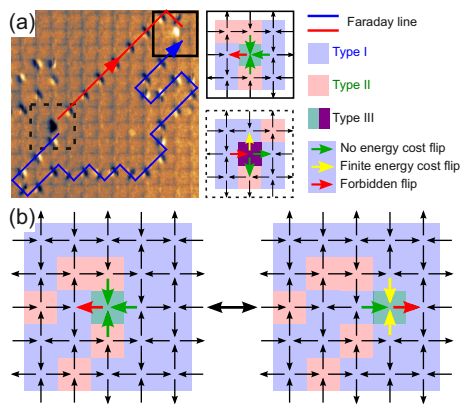

FIG. 5. (a) Two Faraday lines bridged by a pair of ice-rule defects. The schematics on the right side illustrates the local environment of the topological defects and the energy cost associated with a spin flip event. (b) Specific case when propagating the white defect into the type I domain: once the defect has moved into the domain, it is statistically likely that it will be pushed back into the domain wall.

Finally, we emphasize that the strategy proposed in this work has broader applicability than just the F-model and could be applied to other geometries. For example, tuning the vertex energy / hierarchy might be of potential interest in a variety of square based lattices [38], such as the Shakti [39], Tetris [40] or Saint George [41] lattices.

This work was supported by the Agence Na-

tionale de la Recherche through projects no. ANR-17-CE24-0007-03 “Bio-Ice”. The authors acknowledge support from the Nanofab team at the Institut NEEL. CzechNanoLab project LM2018110 funded by MEYS CR is gratefully acknowledged for the financial support of the measurements / sample fabrication at CEITEC Nano Research Infrastructure. The research infrastructure was funded by the Czech Academy of Sciences (project RVO:68081731)

[1] F. E. Simon Zeitschrift für Naturforschung A **6**, 397 (1951).
[2] A. J. Kox Studies in history and philosophy of modern physics **37**, 101 (2006).
[3] A. Y. Klimenko arXiv:1208.4189
[4] W. F. Giauque and M. F. Ashley Phys. Rev. **43**, 81 (1933).
[5] W. F. Giauque and J. W. Stout Journal of the American Chemical Society **58**, 1144 (1936).
[6] J. D. Bernal and R. H. Fowler J. Chem. Phys. **1**, 515 (1933).
[7] L. Pauling J. Am. Chem. Soc. **57**, 2680 (1935).
[8] R. J. Baxter, Exactly solved models in statistical mechanics, Academic Press Limited, London, 1982
[9] E. H. Lieb, Statistical mechanics Springer-Verlag, Berlin, 2004
[10] M. Aizenman and E. H. Lieb J. Statist. Phys. **24**, 279 (1981).
[11] Rys, F. Helvetica Physica Acta **36**, 537 (1963).
[12] E. H. Lieb, Phys. Rev. Lett. **18**, 692-694 (1967).
[13] E. H. Lieb, Phys. Rev. Lett. **18**, 1046 (1967).
[14] E. H. Lieb, Phys. Rev. Lett. **19**, 108-110 (1967).
[15] B. Sutherland, Phys. Rev. Lett. **19**, 103 (1967).
[16] R. J. Baxter, J. Phys. C: Solid State Phys. **6**, L94 (1973).
[17] C. Nisoli, Eur. Phys. Lett. **132**, 47005 (2020).
[18] D. M. Arroo and S. T. Bramwell Phys. Rev. B **102**, 214427 (2020).
[19] C. Nisoli, R. Moessner, and P. Schiffer, Rev. Mod. Phys. **85**, 1473 (2013).
[20] N. Rougemaille and B. Canals, Eur. Phys. J. B **92**, 62 (2019).
[21] S. H. Skjærvø, C. H. Marrows, R. L. Stamps and L. J. Heyderman Nat. Rev. Phys. **2**, 13 (2020).
[22] Wu F. Y., Phys. Rev. Lett., **22**, 1174 (1969).
[23] D. Levis, L. F. Cugliandolo, L. Foini, and M. Tarzia Phys. Rev. Lett., **110**, 207206 (2013).
[24] L. F. Cugliandolo, J. Stat. Phys., **167**, 499 (2017).
[25] O. Sendetskyi, V. Scagnoli, N. Leo, L. Anghinolfi, A. Alberca, J. Lüning, U. Staub, P. M. Derlet, and L. J. Heyderman, Phys. Rev. B **99**, 214430 (2019).
[26] R. F. Wang, C. Nisoli, R. S. Freitas, J. Li, W. McConville, B. J. Cooley, M. S. Lund, N. Samarth, C. Leighton, V. H. Crespi, and P. Schiffer, Nature **439**, 303 (2006).
[27] M. Donahue and D. Porter, Interagency Report NISTIR 6376, National Institute of Standards and Technology, Gaithersburg, MD, 1999.
[28] A. Vansteenkiste, J. Leliaert, M. Dvornik, M. Helsen, and F. Garcia-Sanchez, AIP Advances **4**, 107133 (2014).
[29] Y. Perrin, B. Canals, and N. Rougemaille, Phys. Rev. B **99**, 224434 (2019).
[30] Y. Perrin, B. Canals, and N. Rougemaille, Nature **540**, 410 (2016).
[31] O. Brunn, B. Canals, and N. Rougemaille, Phys. Rev. B **103**, 094405 (2021).
[32] A. Farhan, M. Saccone, C. F. Petersen, S. Dhuey, R. V. Chopdekar, Y.-L. Huang, N. Kent, Z. Chen, M. J. Alava, T. Lippert, A. Scholl, S. van Dijken, Sci. Adv. **5**, eaav6380 (2019).
[33] E. Östman, H. Stopfel, I.-A. Chioar, U. B. Arnalds, A. Stein, V. Kapaklis, B.Hjörvarsson, Nat. Phys.**14**, 375 (2018).
[34] N. Rougemaille and B. Canals, Appl. Phys. Lett. **118**, 112403 (2021).
[35] J. P. Morgan, A. Stein, S. Langridge, and C. H. Marrows, Nat. Phys. **7**, 75 (2011).
[36] J. P. Morgan, A. Bellew, A. Stein, S. Langridge, and C. H. Marrows, Front. Physics **1**, 28 (2013).
[37] J. M. Porro, A. Bedoya-Pinto, A. Berger, and P. Vavassori, New J. Phys. **15**, 055012 (2013).
[38] M. J. Morrison, T. R. Nelson, and C. Nisoli, New J. Phys.**15**, 045009 (2013).
[39] I. Gilbert, G.-W. Chern, S. Zhang, L. O'Brien, B. Fore, C. Nisoli, and P. Schiffer Nat. Phys. **10**, 670 (2014).
[40] I. Gilbert, Y. Lao, I. Carrasquillo, L. O'Brien, J. D. Watts, M. Manno, C. Leighton, A. Scholl, C. Nisoli, and P. Schiffer, Nat. Phys. 12, 162 (2016).
[41] H. Stopfel, U. B. Arnalds, A. Stein, T. P. A. Hase, B. Hjörvarsson, and V. Kapaklis Phys. Rev. Mater. **5**, 114410 (2021).